Unified positional PFEM formulation for fluid-structure interaction problems with free surface flows

G. Avancini[1], S.R. Idelsohn[2,3], R.A.K. Sanches[1]

[1]*Dept. of Structural Engineering, University of São Paulo*
Av. Trabalhador Sãocarlense 400, 13566-590, SP, Brazil
giavancini@usp.br, rodolfo.sanches@usp.br
[2]*ICREA, Catalan Institution for Research and Advanced Studies*
Barcelona, Spain
[3]*CIMNE, International Centre for Numerical Methods in Engineering*
Barcelona, Spain
sergio@cimne.upc.edu

Abstract. This paper aims to present a positional unified PFEM formulation to solve problems of free surface flows interacting with elastic structures. In contrast with traditional FEM formulations of fluid mechanics that use velocities, here we use nodal position as the main variables for both solid and fluid. In addition, the same solution scheme is used to solve the governing equations of both physical problems. In fact, the coupled problem is treated as an unique spatial domain containing two different materials. For the solid, a hyperelastic Saint-Venant-Kirchhoff model is adopted, which is suited for large displacement analysis within the small strain regime, while the fluid is considered to have an incompressible-Newtonian behavior. A mixed position-pressure approximation is adopted for the fluid domain to ensure incompressibility, together with a Pressure Stabilizing Petrov-Galerkin (PSPG). The time marching procedure is performed by means of the second order alpha-generalized scheme. The usage of a Lagrangian description naturally allows the simulation of deformable solids and free surface flows as the movement of the mesh nodes coincides with the physical particles motion. However, free surface flows tend to deteriorate the mesh quality as topological changes and several distortions of the fluid domain may occur. To deal with that, the PFEM plays a key role by constantly regenerating the mesh and automatically detecting the physical boundaries by combining an efficient Delaunay triangulation-alpha-shape procedure. The applicability of the developed approach is demonstrated by the simulation of selected problems.

Keywords: PFEM, Fluid-Structure Interaction, Free Surface Flow, Unified Formulation

1 Introduction

Fluid-Structure interaction (FSI) problems with free surface flows challenge the numerical methods as they typically involve large distortions in the domain and could also present topological changes.

To overcome the limitations of using an Eulerian description with fixed mesh for the fluid, two main classes of methods emerged: the interface tracking and interface capturing methods. In the first group, the mesh moves to track the fluid-structure interface movement. As a consequence, the mesh can become too distorted if the interface undergoes large displacements. The ALE description, introduced by Donea et al. [1] and the space-time formulation, proposed by Tezduyar et al. [2], are examples of interface tracking methods. On the other hand, the interface capturing methods are based generally on non-moving meshes, on which the free surface position is determined by solving an additional advection equation. The contributions of the structure to the fluid problem are then accounted for by means of Immersed Boundary techniques, as described by Peskin [3].

Alternatively, using a Lagrangian framework also for the fluid, the free surface shape is naturally known by the particles or mesh nodes position. Furthermore, the coupling becomes simplified once the movement of both domains are described using the same mathematical description. The difficulty is then transferred to a way of keeping the mesh quality throughout the analysis.

Thinking on that, Idelsohn et al. [4] and Oñate et al. [5] developed an innovative numerical method called Particle Finite Element Method (PFEM). In the PFEM, the mesh is frequently reconstructed over a set of particles by means of the Delaunay triangulation, and the physical boundary is identified using the geometric criteria α-shape. Thanks to that, the method makes possible the simulation of really complex problems, such as free surface flows (Idelsohn et al. [6]), melting solids (Onate et al. [7], Franci et al. [8]), soil excavation (Carbonell et al. [9]) among others.

2 Fluid dynamics problem

The equilibrium equation of an incompressible Newtonian flow is here obtained applying the Principle of Stationary Potential Energy and integrating over the last known configuration Ω_n, which reads:

$$\begin{aligned}\frac{\partial \Pi^h}{\partial \boldsymbol{x}^a} = \int_{\Omega_n} \rho_n \ddot{\boldsymbol{x}}^h N^a dv_n + \int_{\Omega_n} \mathbf{S'}^h : \frac{\partial \mathbf{E}^h}{\partial \boldsymbol{x}^a} dv_n + \int_{\Omega_n} p^h J^h \mathbf{C}^{-1\,h} : \frac{\partial \mathbf{E}^h}{\partial \boldsymbol{x}^a} dv_n \\ - \int_{\Omega_n} \mathbf{b}_n N^a dv_n - \int_{\partial\Omega_n} \mathbf{t}_n N^a ds_n = \mathbf{0},\end{aligned} \tag{1}$$

$$\frac{\partial \Pi^h}{\partial p^a} = \int_{\Omega_n} N^a \left(J^h - 1\right) dv_n = 0. \tag{2}$$

In the above equations, $\boldsymbol{x}^a$, p^a and N^a is the vector of positions, the pressure and the shape function of a node a, $\mathbf{S'}$ is the deviatoric Piola-Kirchhoff stress tensor, $\mathbf{E}$ is the Green-Lagrange strain tensor, $\mathbf{C}^{-1}$ is the inverse of the right Cauchy-Green tensor, J is the jacobian of the deformation gradient $\mathbf{F}$, $\mathbf{b}_n$ is the body forces, $\mathbf{t}_n$ is the surface traction and the superscript h indicates an interpolated variable. The positions and pressures are approximated using equal-order linear shape functions.

The Piola-Kirchhoff stress tensor is written in terms of the Green-Lagrange strain rate as

$$\mathbf{S'} = \mathfrak{D}_n : \dot{\mathbf{E}}, \tag{3}$$

where $\dot{\mathbf{E}}$ is the Green-Lagrange strain rate and $\mathfrak{D}_n$ represents the constitutive tensor related to the reference configuration, given by

$$(\mathfrak{D}_r)_{ijkl} = J F^{-1}_{ia} F^{-1}_{jb} F^{-1}_{kc} F^{-1}_{ld} \mathfrak{D}_{abcd}, \tag{4}$$

with $\mathfrak{D}_{abcd}$ standing for the constitutive tensor related to the current configuration, which is dependent of the viscosity by the law:

$$\mathfrak{D} = \mu \left(\mathbf{I} \otimes \mathbf{I} + \mathbf{I} \otimes \mathbf{I}\right). \tag{5}$$

When using equal-order interpolation for both position and pressure, it is necessary to stabilize the equation (2) in order to obtain a good distribution for the pressure. For this purpose, we use the Pressure Stabilizing Petrov-Galerkin (PSPG), proposed by Tezduyar [10], that adds to the incompressibility equation a term based on the momentum residual scaled by the parameter τ_{PSPG}:

$$\begin{aligned}\int_{\Omega_n} N^a \left(J^h - 1\right) dv_n + \int_{\Omega_n} \tau_{PSPG} \nabla_n N^a \mathbf{F}^{-1\,h} \ddot{\boldsymbol{x}}^h dv_n - \\ \int_{\Omega_n} \frac{\tau_{PSPG}}{\rho_n} J^h \nabla_n N^a \mathbf{C}^{-1\,h} \nabla_n p^h dv_n - \int_{\Omega_n} \frac{\tau_{PSPG}}{\rho_n} \nabla_n N^a \mathbf{F}^{-1\,h} \mathbf{b}_n dv_n = 0.\end{aligned} \tag{6}$$

The equations (1) and 6 are integrated in time using the α generalized method. For a more detailed explanation of the formulation presented here, the readers should refer to Avancini and Sanches [11].

2.1 The Particle Finite Element Method

The key point in the PFEM is the mesh generation procedure, which combines the Delaunay triangulation over the physical particles and the α-shape method. This last technique is used to erase those simplices that are too distorted or too big based on a geometrical criteria. For each element e, we compare its circumradius r_e with the initial mean mesh size h_e scaled by a α parameter. If the condition

$$r_e > \alpha h_e, \tag{7}$$

holds, the element is erased. By doing this, the external boundaries can be identified, and it allows even the fragmentation of the domain, representing for instance, water drops. For more information about the PFEM, we suggest the readers to refer to Idelsohn et al. [4], Franci [12] and Avancini [13].

3 Solid dynamics problem

Very similar to the fluid, the solid equilibrium is also obtained through the Principle of Stationary Potential Energy, however, for compressible solids it is not necessary to split the internal energy, and the initial configuration is adopted as the reference configuration. Thus, one writes:

$$\begin{aligned}\frac{\partial \Pi^h}{\partial \boldsymbol{x}^a} = \int_{\Omega_0} \rho_0 \ddot{\boldsymbol{x}}^h N^a dv_0 + \int_{\Omega_0} \mathbf{S}^h : \frac{\partial \mathbf{E}^h}{\partial \boldsymbol{x}^a} dv_0 - \int_{\Omega_0} \mathbf{b}_0 N^a dv_0 \\ - \int_{\partial\Omega_0} \mathbf{t}_0 N^a ds_0 = 0.\end{aligned} \tag{8}$$

Linear shape functions are used for the positions. In order to represent the material behavior, we use the Saint-Venant-Kirchhoff hipereslatic model. It formulates a linear relation between the Piola Kirchhoff stress tensor and the Green-Lagrange strain tensor as:

$$\mathbf{S} = \mathfrak{D} : \mathbf{E}, \tag{9}$$

where the fourth order constitutive tensor $\mathfrak{D}$ is given by

$$\mathfrak{D} = \lambda \mathbf{I} \otimes \mathbf{I} + \mathbf{2G}\mathbf{II}. \tag{10}$$

In the equation above, λ is a material parameter known as Lame constant, $\otimes$ indicates the tensor product, G is the transversal Young modulus and $\mathbf{II}$ is the fourth order identity tensor.

4 Monolithic coupling strategy

The coupling between the fluid and the structure is performed in a monolithic way, which means that both domains are solved in an unique system of equations. Also, we assume that the meshes are conform at the interface, or in other words, the fluid nodes must be coincident with the solid ones at the interface.

Bearing in mind that the interface nodes receive contribution from both fluid and solid elements to the positions degrees of freedom, and only from fluid elements to the pressure degrees of freedom, the system matrix can be assembled as follows:

$$\begin{bmatrix} [\mathbf{M}]_f & [\mathbf{M}]_f & 0 & [\mathbf{M}]_f & [\mathbf{M}]_f \\ [\mathbf{M}]_f & [\mathbf{M}]_f & 0 & [\mathbf{M}]_f & [\mathbf{M}]_f \\ 0 & 0 & [\mathbf{M}]_s & [\mathbf{M}]_s & 0 \\ [\mathbf{M}]_f & [\mathbf{M}]_f & [\mathbf{M}]_s & [\mathbf{M}]_f + [\mathbf{M}]_s & [\mathbf{M}]_f \\ [\mathbf{M}]_f & [\mathbf{M}]_f & 0 & [\mathbf{M}]_f & [\mathbf{M}]_f \end{bmatrix} \begin{Bmatrix} \Delta \boldsymbol{x}_f \\ \Delta \boldsymbol{p}_f \\ \Delta \boldsymbol{x}_s \\ \Delta \boldsymbol{x}_{fs} \\ \Delta \boldsymbol{p}_{fs} \end{Bmatrix} = - \begin{Bmatrix} \boldsymbol{r}_{mf} \\ \boldsymbol{r}_{cf} \\ \boldsymbol{r}_{ms} \\ \boldsymbol{r}_{mf} + \boldsymbol{r}_{ms} \\ \boldsymbol{r}_{cf} \end{Bmatrix}, \tag{11}$$

with the subscripts f, s e fs standing for a quantity related to the fluid domain, solid domain or to the fluid-structure interface, $\Delta \boldsymbol{x}$ and $\Delta \boldsymbol{p}$ represent the increment of position and pressure, respectively, and lastly, $\boldsymbol{r}_m$ and $\boldsymbol{r}_c$ are the residuals of momentum and incompressibility equations.

5 Numerical examples

Two numerical fluid-structure interaction problems are presented in this section. High complex phenomena are involved in these problems, such as topological changes, wave breaking, hydrodynamic impact, fluid domain separation and the formation of water drops. In both cases, a value of $\alpha = 1.2$ is used for the α-shape method, and the spectral radius is set to $\rho_\infty = 0.9$.

5.1 Dam break over an elastic obstacle

The first case is a benchmark of a dam break over an elastic obstacle, firstly proposed by Walhorn et al. [14]. The right wall is instantly removed at the beginning of the analysis, setting the water mass to flow and impact on a flexible membrane which starts to oscillate. The initial geometry is depicted on Fig. 1, where $L = 0.146$ m, $D = 0.012$ m and $H = 0.08$ m. The viscosity and density of the fluid were assumed equal to $\mu = 0.001$ Pa·s and $\rho_f = 1000.0$ kg/m^3, while for the solid, a young modulus $E = 10^6$ Pa, poison ratio 0.0 and density $\rho_s = 2500.0$ kg/m^3 were used. The gravity acceleration $g = 9.81$ m/s^2 acts downwards only on the fluid domain and stick conditions were applied on the rigid walls, so the normal and tangential components of displacements were set to zero in a strong manner.

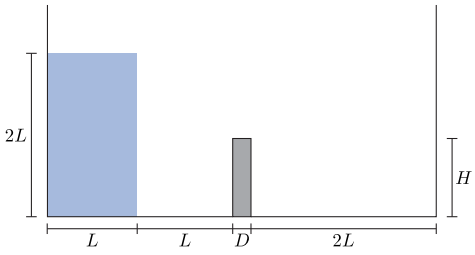

Figure 1. Dam break over an elastic obstacle. Initial geometry

The analysis was carried out using two different meshes. The coarser one has a characteristic length $h_e = 0.004$ m, 6154 fluid elements and 120 solid elements, while the finer mesh has $h_e = 0.003$ m, 10886 fluid elements and 208 solid elements. The problem was simulated for a total of 1.0 s, with a time step $\Delta t = 0.001$ s for both meshes.

The horizontal displacement of the membrane's tip was monitored and one can see a comparison to the numerical results from Walhorn et al. [14] and Idelsohn et al. [15] in Fig. 2. For the first part of the analysis, the results from both meshes agree well with the references, especially with Walhorn et al. [14]. After 0.5 s, the structural response of all formulations starts to diverge. From this point, a series of complex phenomena, like splashes and volume separation, can be observed and it highly affects the wave formation and consequently, the time that the flow impacts the structure right side. These mechanisms seem to be dependents of the choice of the α-shape parameter and the characteristic length of the mesh. Furthermore, the membrane's flexibility plays a key role in the second part of the analysis. In the case where the structure presents a smaller displacement peak value, the fluid mass impacts on the right rigid wall at a taller point and with higher tangential velocity, thus delaying the wave formation and the subsequent impact on the structure.

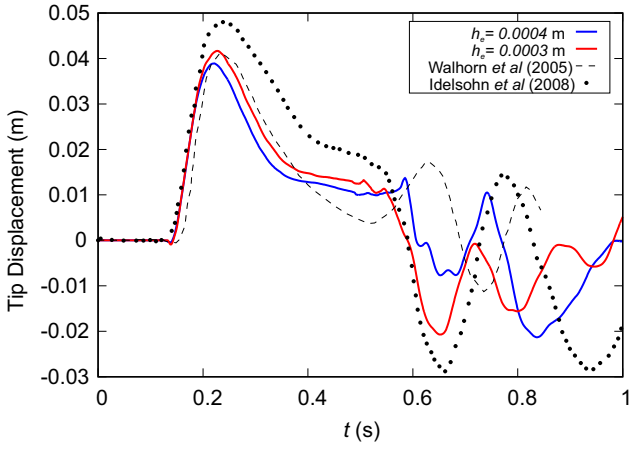

Figure 2. Dam break over an elastic obstacle. Tip horizontal displacement

Figure 3 contains some snapshots of the free surface shape and the stress distribution over the deformed structure using the finer mesh. Qualitatively, the results are in accordance with the physics of the problem, and one can see that the formulation is capable of representing the complex events involved in this simulation: topological changes in the fluid domain, water impact, breaking waves and large displacements.

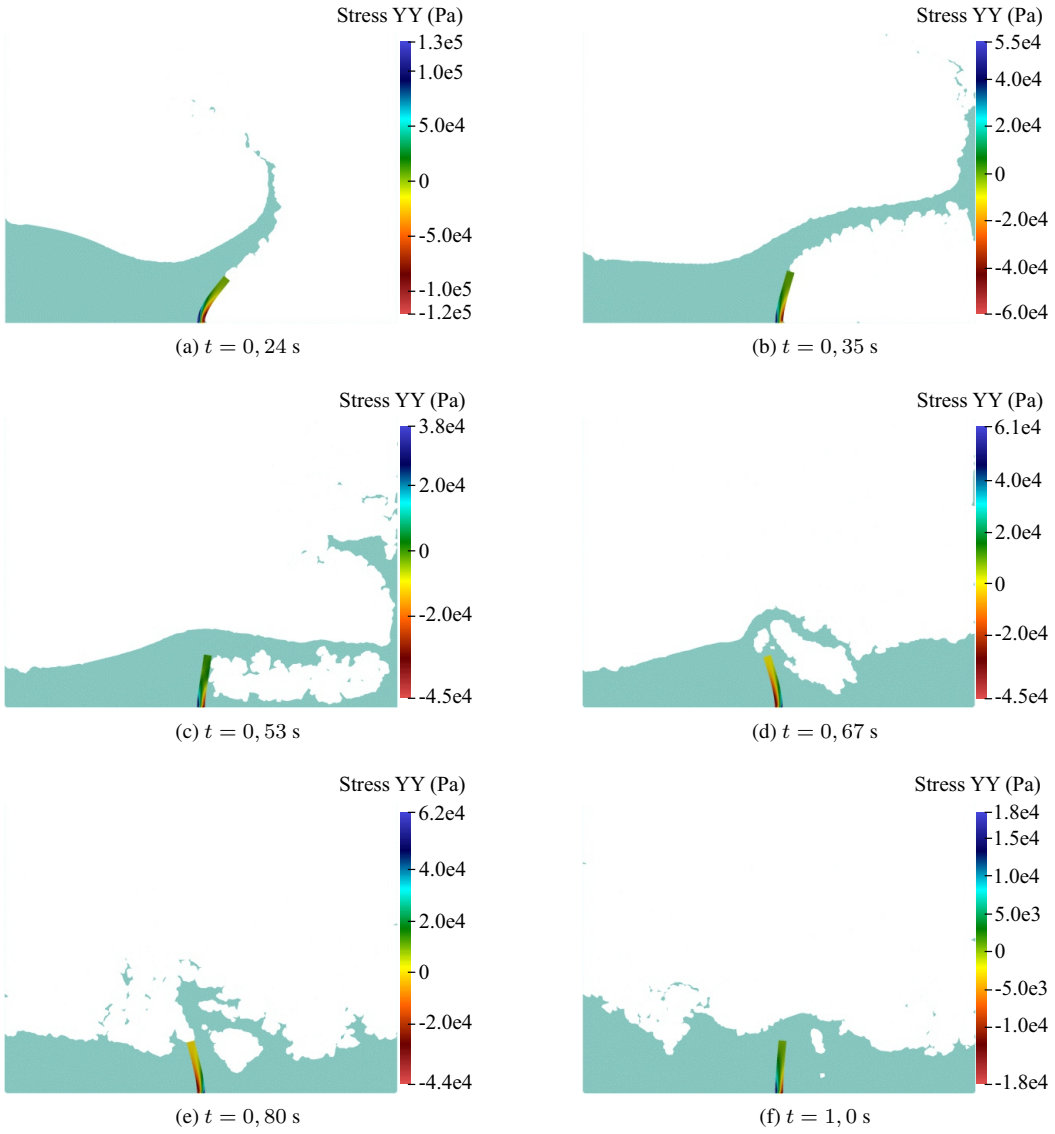

(a) $t = 0,24$ s (b) $t = 0,35$ s

(c) $t = 0,53$ s (d) $t = 0,67$ s

(e) $t = 0,80$ s (f) $t = 1,0$ s

Figure 3. Dam break over an elastic obstacle. Snapshots of the free surface shape and structure stress distribution

5.2 Filling of a flexible container with viscous fluid

This example can be seen in the work of Franci [12] and consists of a highly flexible container being filled with a viscous fluid that lays in a conic tank. The initial geometry is depicted in Fig. 4a, where $B = 4.4714$ m, $b = 1.3$ m, $h = 2.5$ m, $l = 3.75$ m, $t = 0.2$ m e $r = 2.25$ m. Due to the impact of the fluid mass, the container suffers a severe stretch and starts to oscillate, which in turn affects the fluid flow, thus presenting a strong coupling. A case of a very viscous fluid with $\mu = 50.0$ Pa·s and $\rho_f = 1000.0$ kg/m^3 was considered, and the solid was assumed to have $E = 2.1 \cdot 10^7$ Pa, $\nu = 0.3$ and $\rho_s = 20.0$ kg/m^3. The gravity $g = 9.81$ m/s^2 acts only on the fluid, stick conditions were applied on the tank walls and the problem was simulated for 10.0 s using a time step $\Delta t = 0.001$ s.

Two different meshes were used to discretize the domain: the first one has a size $h_e = 0.1$ m, 1007 fluid elements and 568 solid elements, while the second one has a characteristic length $h_e = 0.05$ m with 7231 fluid elements and 2646 solid elements. Firstly, the vertical displacement of the bottom of the elastic container was monitored and compared to the reference. One can observe in Figure 4b a good agreement with the results from Franci [12], especially during the first 3 s of analysis. After that, as mentioned in the previous example, a series of events that are very sensitive to mesh refinement and to the α-shape parameter starts to affect the solution. Using a coarser mesh implies in a less flexible structure, leading to a small amplitude oscillation. On the other hand, the solution obtained with the finer mesh shows a higher amplitude of vibration. For both cases, the structure oscillates

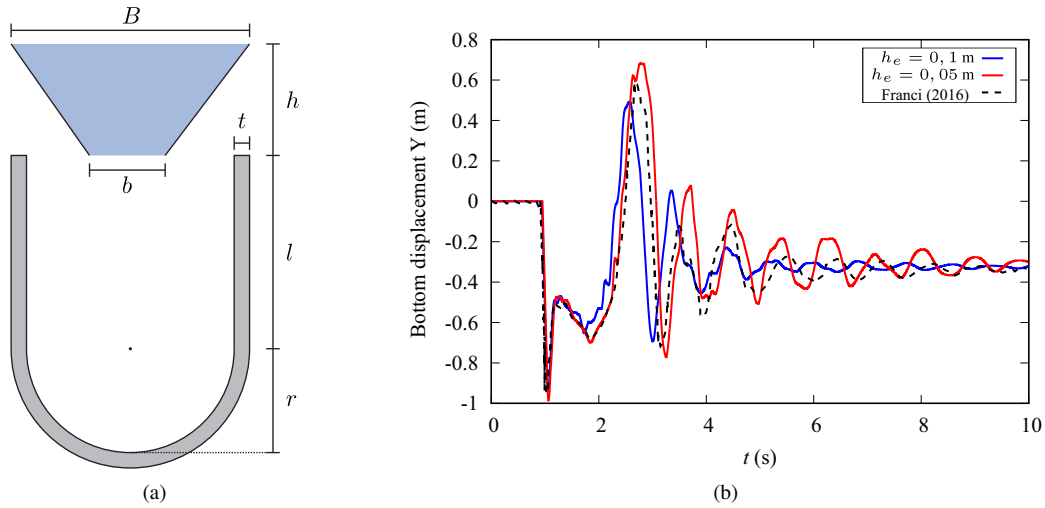

Figure 4. Filling of a flexible container with viscous fluid. (a) Initial geometry and (b) Vertical displacement of the bottom of the elastic container

ten times during 10 s of simulation, which is in agreement with Franci [12]. Some snapshots of the free surface shape and the stress field of the container can be seen in Figure 5. Again, one can observe that the results are in accordance with the physics of the problem.

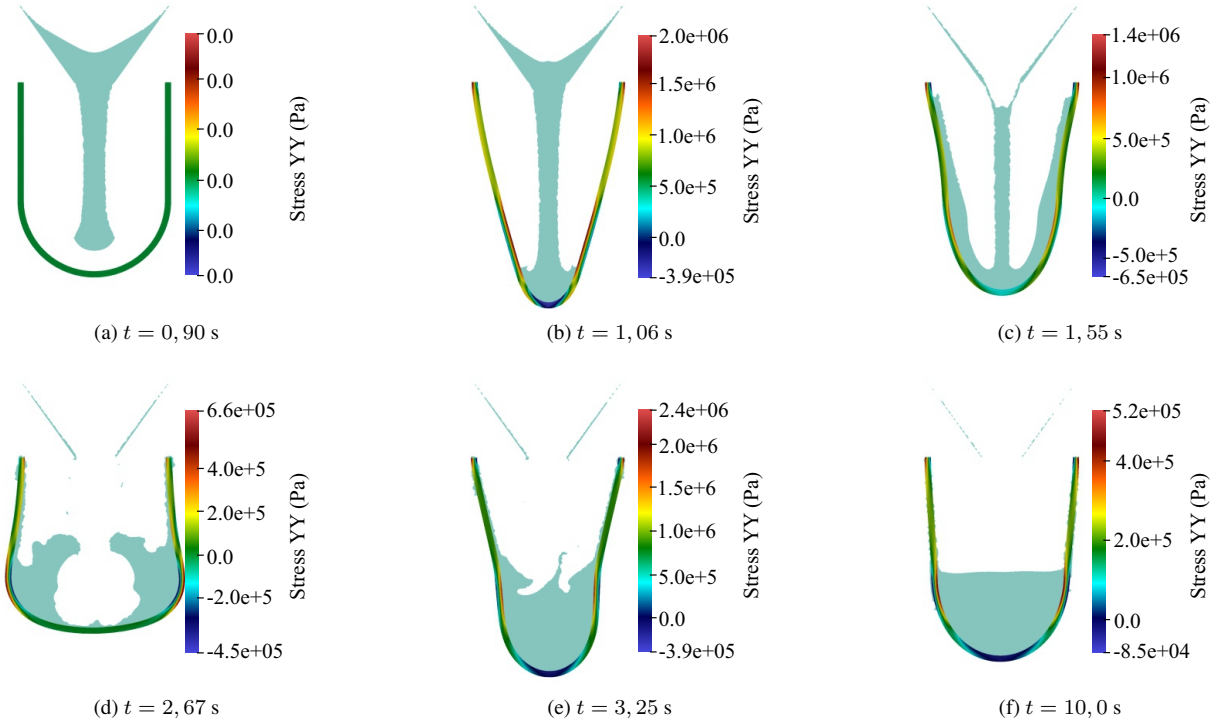

Figure 5. Filling of a flexible container with viscous fluid. Snapshots of the free surface shape and stress field of the structure

6 Conclusions

In this paper, an unified PFEM formulation based on positions was developed and two fluid-structure interaction problems with free surface flow were presented. Due to the fact that we use the same variables, same

description, and same solution scheme for both materials, the monolithic coupling strategy becomes straightforward to be implemented, and ended up being very robust for the simulation of strongly coupled problems. In fact, one can simulate FSI problems just by summing the contributions for both materials at the interface degrees of freedom during the system matrix assemble.

The results shown in this work also demonstrate the versatility and applicability of the PFEM. By combining a robust Delaunay triangulation with the α-shape method to identify the external boundaries, it becomes possible to handle very large domain distortions, topological changes and even domain separations, making it ideal for the simulation of free surface flows.

Acknowledgements. This study was financed in part by the Coordination for the Improvement of Higher Education Personnel – Brasil (CAPES) – Finance Code 001 and by the Brazilian National Council for Research and Technological Development (CNPq) - grants 88887.577322/2020-00 and 141804/2018-1

Authorship statement. The authors hereby confirm that they are the sole liable persons responsible for the authorship of this work, and that all material that has been herein included as part of the present paper is either the property (and authorship) of the authors, or has the permission of the owners to be included here.

References

[1] J. Donea, S. Giuliani, and J.-P. Halleux. An arbitrary lagrangian-eulerian finite element method for transient dynamic fluid-structure interactions. *Computer methods in applied mechanics and engineering*, vol. 33, n. 1-3, pp. 689–723, 1982.

[2] T. Tezduyar, M. Behr, and J. Liou. A new strategy for finite element computations involving moving boundaries and interfaces—the deforming-spatial-domain/space-time procedure: I. the concept and the preliminary numerical tests. *Computer Methods in Applied Mechanics and Engineering*, vol. 94, n. 3, pp. 339 – 351, 1992.

[3] C. S. Peskin. The immersed boundary method. *Acta numerica*, vol. 11, pp. 479–517, 2002.

[4] S. R. Idelsohn, E. Oñate, and F. D. Pin. The particle finite element method: a powerful tool to solve incompressible flows with free-surfaces and breaking waves. *International journal for numerical methods in engineering*, vol. 61, n. 7, pp. 964–989, 2004.

[5] E. Oñate, S. R. Idelsohn, F. Del Pin, and R. Aubry. The particle finite element method—an overview. *International Journal of Computational Methods*, vol. 1, n. 02, pp. 267–307, 2004.

[6] S. Idelsohn, J. Marti, A. Souto-Iglesias, and E. Oñate. Interaction between an elastic structure and free-surface flows: experimental versus numerical comparisons using the pfem. *Computational Mechanics*, vol. 43, n. 1, pp. 125–132, 2008a.

[7] E. Onate, R. Rossi, S. R. Idelsohn, and K. M. Butler. Melting and spread of polymers in fire with the particle finite element method. *International journal for numerical methods in engineering*, vol. 81, n. 8, pp. 1046–1072, 2010.

[8] A. Franci, E. Oñate, J. M. Carbonell, and M. Chiumenti. Pfem formulation for thermo-coupled fsi analysis. application to nuclear core melt accident. *Computer Methods in Applied Mechanics and Engineering*, vol. 325, pp. 711–732, 2017.

[9] J. M. Carbonell, E. Oñate, and B. Suárez. Modeling of ground excavation with the particle finite-element method. *Journal of engineering mechanics*, vol. 136, n. 4, pp. 455–463, 2010.

[10] T. E. Tezduyar. Stabilized finite element formulations for incompressible flow computations. *Advances in applied mechanics*, vol. 28, pp. 1–44, 1991.

[11] G. Avancini and R. A. Sanches. A total lagrangian position-based finite element formulation for free-surface incompressible flows. *Finite Elements in Analysis and Design*, vol. 169, 2020.

[12] A. Franci. *Unified Lagrangian formulation for fluid and solid mechanics, fluid-structure interaction and coupled thermal problems using the PFEM*. Springer, 2016.

[13] G. Avancini. Análise numérica bidimensional de interação fluido-estrutura: uma formulação posicional baseada em elementos finitos e partículas. Mestrado, SET-EESC-USP, São Carlos, São Paulo, Brasil, 2018.

[14] E. Walhorn, A. Kölke, B. Hübner, and D. Dinkler. Fluid–structure coupling within a monolithic model involving free surface flows. *Computers & structures*, vol. 83, n. 25-26, pp. 2100–2111, 2005.

[15] S. R. Idelsohn, J. Marti, A. Limache, and E. Oñate. Unified lagrangian formulation for elastic solids and incompressible fluids: application to fluid–structure interaction problems via the pfem. *Computer Methods in Applied Mechanics and Engineering*, vol. 197, n. 19-20, pp. 1762–1776, 2008b.